Combinatorial screening for specific drug solubilizers with switchable release profiles

Wieczorek, Sebastian; Vigne, Sara; Masini, Tiziana; Ponader, Daniela; Hartmann, Laura; Hirsch, Anna K H; Börner, Hans G

Published in:
Macromolecular Bioscience

DOI:
10.1002/mabi.201400443

Publication date:
2015

Combinatorial Screening for Specific Drug Solubilizers with Switchable Release Profiles[a]

Sebastian Wieczorek, Sara Vigne, Tiziana Masini, Daniela Ponader, Laura Hartmann, Anna K. H. Hirsch, Hans G. Börner*

Polymer-*block*-peptide conjugates are tailored to render hydrophobic small molecule drugs water soluble. The combinatorial strategy selects for bioconjugates that exhibit sequence-specific solubilization and switchable release profiles of the cargo through incorporation of a disulfide linker moiety into the peptide-library design. While the study focused on the photosensitizer *m*-THPC and reductive carrier cleavage, the approach is generic and might be expanded toward a broad range of poorly soluble small-molecule drugs and other selective cleavage mechanisms to disassemble a peptide binding domain of the bioconjugate-based solubilizer.

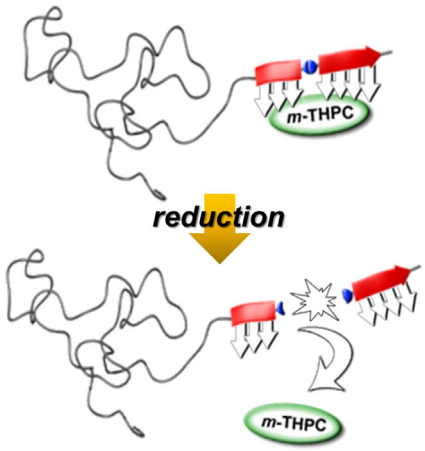

1. Introduction

Nowadays, the majority of novel small-molecule lead compounds in pharmaceutical research are identified by high-throughput screening or structure-based design.[1–6] Frequently, these lead compounds suffer from restrictions in application and approval due to unfavorable properties such as low water solubility or disfavored precipitation in biological environments.[1] Poor water solubility of lead compounds results often in low bioavailability and is one of the key difficulties in drug development, hampering drug potency, and approval.[7] Means to overcome these drawbacks are frequently time- and cost-intensive as they include consecutive structure adaptation and optimization cycles.[8,9] Modification of the original drug structure might go along with the inherent risk of jeopardizing the drug activity and potentially lead to structure failure. Several alternative strategies to achieve solubilization of water-insoluble, high-potential compounds have been

S. Wieczorek, Prof. H. G. Börner
Laboratory for Organic Synthesis of Functional Systems, Department of Chemistry, Humboldt-Universität zu Berlin, Brook-Taylor-Str. 2, D-12489, Berlin, Germany
E-mail: h.boerner@hu-berlin.de
Fax: +49 (0)30 2093-7500
S. Vigne
École Polytechnique Fédérale de Lausanne (EPFL), Institute of Materials (IMX), EPFL – STI – IMX – LMOM, MXG 037, Station 12, CH-1015, Lausanne, Switzerland
T. Masini, Dr. A. K. H. Hirsch
Stratingh Institute for Chemistry, University of Groningen, Nijenborgh 7, NL-9747 AG, Groningen, The Netherlands
Dr. D. Ponader, Prof. L. Hartmann
Max Planck Institute of Colloids and Interfaces, MPI KGF Golm, D-14424, Potsdam, Germany

[a]**Supporting Information** is available online from the Wiley Online Library or from the author.

DOI: 10.1002/mabi.201400443

investigated. For instance, drug formulation utilizing synthetic polymers have proven to enable drug delivery of active compounds,[10] increased half-life times,[11] or achieve even passive targeting.[12,13] Particularly block copolymers were exploited intensively to bind and transport poorly soluble small-molecule drugs by non-covalent interactions.[14] The transport and release of drug cargo should ideally be as controlled as possible to maintain the concentration of active drug in the targeted region in a specific window. Most common systems for drug delivery are reservoir and matrix systems, but these cannot be easily tuned.[15] More advanced release systems use triggered delivery upon external stimuli such as pH,[16] enzyme activity,[17] or light.[18] Such behavior can be realized by implementing cleavable moieties in block copolymers, where degradation could be triggered, for instance by hydrolysis of ester bonds, enzymatic proteolysis of peptide bonds,[19] photo-activated cleavage,[20] or reductive disulfide cleavage.[21,22]

During the last decade, polymer–peptide conjugates have demonstrated high potential for materials sciences and biomedical applications.[23–32] Polymer–peptide conjugates provided for instance a precise platform for tuning interaction capabilities and are therefore suitable to be exploited as specific drug solubilizers as well as advanced drug-transport systems.[33] Peptide–poly(ethylene oxide) conjugates (peptide–PEO conjugates) enabled sequence-specific solubilization of inhibitors of the kinase IspE.[34] Additionally, a combinatorial means was described, enabling the selection of drug-binding peptides by screening large peptide libraries.[35] Peptide–PEO conjugates could be selected for *m*-tetra(hydroxyphenyl) chlorin (*m*-THPC), which constitutes a chlorin-based photosensitizer, utilized for photodynamic cancer therapy (PDT). *m*-THPC was effectively solubilized, generating an inactive, silent transport form, which activates in definable rates by trans-solubilization of the cargo to plasma protein models. *m*-THPC is certainly a promising drug candidate, which is even partially approved for treatment of head and neck squamous cell carcinoma.[36,37] However, water insolubility and strong tendency to self-quenching limit the clinical applicability and unfavored partitioning might result in light sensitivity of the patients over several days.[38]

Here, we describe the extension of a combinatorial screening strategy to select specific solubilizers for difficult small-molecule drugs by implementing programmed decomposition to actively enhance the cargo release by reductive external triggers. For that purpose, an unnatural amino acid building block exhibiting a disulfide bond was integrated into a one-bead/one-component peptide library.[39,40] The disulfide bond was located in the main chain and potentially enabled the reductive cleavage in the intracellular environment of a cell. Carrier decomposition affects the trans-solubilization rates and thus the activation kinetics of the *m*-THPC cargo.

2. Experimental Section

Materials, instrumentation, experimental procedures, and analytical data are available in the Supporting Information (S.I.).

3. Results and Discussion

3.1. Peptide Library Design

To obtain a tailor-made peptide–PEO conjugate that specifically solubilizes *m*-THPC and enables programmed decomposition by an external reductive trigger to modulate drug-activation kinetics, an integrated combinatorial approach was applied. The incorporation of a cleavable building block into described *m*-THPC binding domains[35] might alter drug binding in an unpredictable manner. Therefore, a new peptide library was established and an Fmoc-protected unnatural amino acid (Fmoc-Cystaminsuccinate, CDS, c.f. S.I.) containing the disulfide linker was incorporated (cf. S.I.).[39,40] Combinatorial split & mix procedures were used to synthesize a 7mer peptide library (cf. Figure 1).[35,41] A previous study on *m*-THPC peptide binders indicated the importance of the aromatic residue Phe, whereas polar, uncharged Ser and conformationally flexible Gly were less relevant.[35] The second-generation one bead/one component peptide library should elucidate more accurately the importance of aromatic residues by integrating Phe, Tyr, and Trp residues. Moreover, the hydrophobic Leu, the polar neutral Gln, the cationic Arg, and the anionic Glu residues were altered on each of the seven amino acid positions, comprising a set of 8.2×10^5 different amino acid sequences. The disulfide linker moiety was placed at one distinct position in-between the Axx4 and Axx5 in every peptide sequence. Upon reductive cleavage of the disulfide the peptide fragments and thus decreases the affinity for the drug cargo (Figure 1). The variable 7mer sequence section of the library was C-terminally extended with a non-altered Gly-Gly-Met segment. This enables cyanogen bromide cleavage for ease of analysis and a Gly-Gly motif was inserted to space the binding sequence from the support backbone.

After synthesizing the peptide library with split & mix strategy by applying Fmoc bench-top protocols and full deprotection, the library was incubated with *m*-THPC in 10% ethanolic solution. The drug enrichment on certain beads that present suitable peptide sequence for *m*-THPC complexation was followed by fluorescence microscopy using the excitation of the intrinsic fluorescence of the drug moiety at 654 nm (cf. S.I. Figure S1). Clearly, a fraction of the supports exhibited a pronounced fluorescence after incubation. This distinguishable pool was separated by hand sorting. The peptides on those isolated beads were liberated by cyanogen bromide cleavage[42] and the amino acid sequences were analyzed by MALDI-ToF-MS/MS peptide sequencing.[35,43]

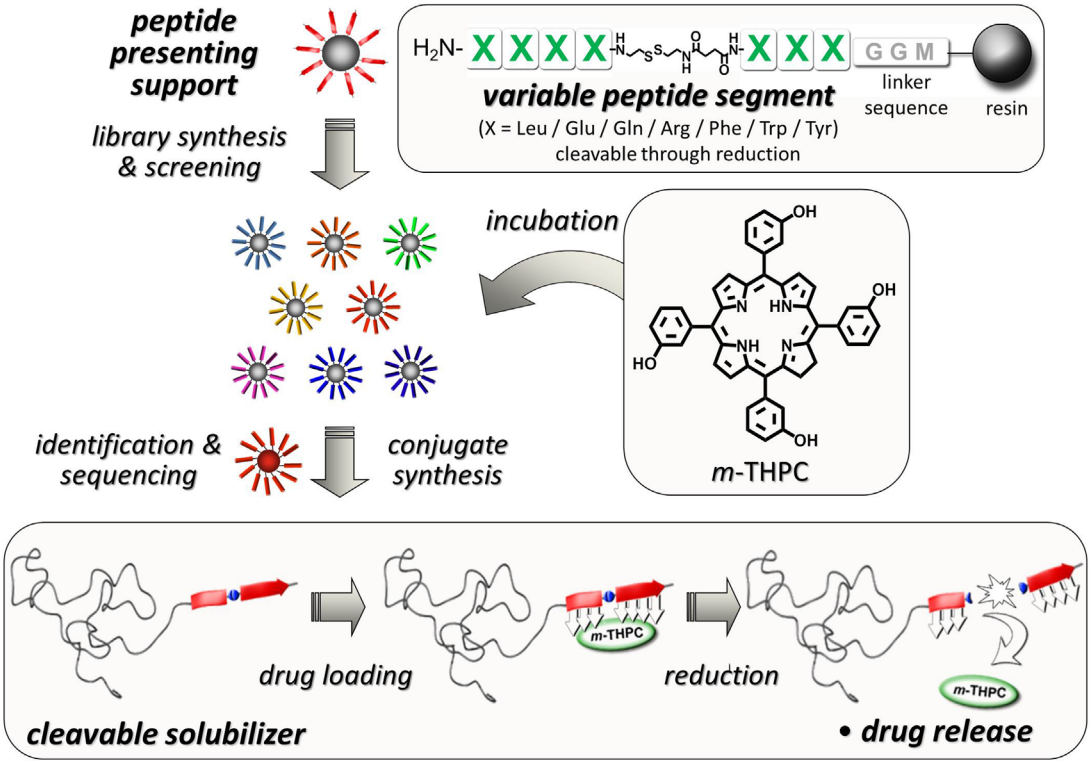

Figure 1. Schematic representation of the screening procedure, involving design and synthesis of a peptide library presenting peptides on solid supports, partitioning of *m*-THPC drug in those libraries, hand selection and ms/ms sequencing to give a set of peptide sequences (left) followed by the synthesis of peptide–PEO conjugate solubilizers, which can be used to study drug loading and cleavage of the peptide segments via reductive means to stimulate drug release (bottom).

3.2. Peptide Sequencing

The set of obtained sequences is summarized in the S.I. (Table S1). A global amino acid analysis revealed the importance of aromatic amino acids, as Phe, Tyr, and Trp are prevalent. This is to be expected taking the highly aromatic structure of *m*-THPC into account. The fine analysis indicated that Phe as most unpolar aromatic amino acid is the dominating residue in all positions of the selected sequence set. In the variable C-terminal 3mer sequence between the disulfide linker and the polar ChemMatrix polymer support, practically all other amino acids are suppressed by the aromatic residues (cf. S.I. Figure S2). At the N-terminal 4mer sequence, polar non-ionic and negatively charged residues are dominating compared to the C-terminal 3mer region. This is particularly obvious for sequence positions close to the N-terminus, as negatively charged Glu is enriched at the N-terminal position Axx1. Closer to the disulfide linker, the polar, non-ionic Gln occurs more frequently. Furthermore, the hydrophobic, non-aromatic Leu becomes more prominent in the middle of the 4mer segment on position Axx2–Axx4 as it seems to be required for hydrophobic contacts with the *m*-THPC. Arg was rarely found, leading to the assumption that positively charged amino acids are not required for *m*-THPC binding.

From the sequence set two peptides were more deeply investigated. The sequences are in good agreement with previously found *m*-THPC peptide-based binding domains and represent a combination of obviously relevant residues Phe, Leu, and Glu at preferential sequence positions.[35] The peptides were synthesized as peptide-PEO conjugates by semi-automated solid-phase peptide synthesis (SPPS) on a PEO preloaded PAP-Resin (polystyrene attached PEO resin) using adapted FastMoc protocols (cf. Figure 2, **PI**, **PII**). Where **PI** is composed of a C-terminal Phe trimer and an N-terminal tetramer sequence (LWQY), **PII** is slightly less aromatic with only four aromatic residues, but has with three Leu residues a higher content of hydrophobic, aliphatic amino acids. After synthesis was completed, the bioconjugates could be cleaved from the supports, deprotected and the chemical identities were confirmed by MALDI-Tof MS and NMR analysis (cf. S.I.).

3.3. Drug Solubilization

The carriers were readily soluble in water at pH 7.0 and could be investigated for solubilization efficiency and payload capacity. The bioconjugates were loaded in water with the maximal amount of *m*-THPC by utilizing the

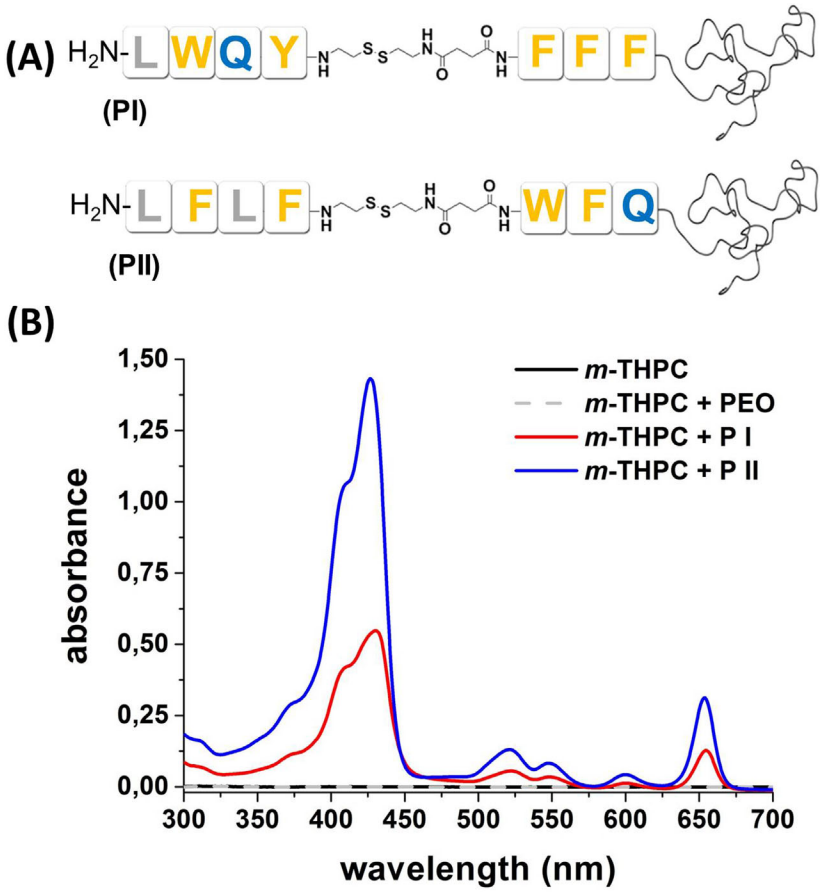

Figure 2. Selected peptide–PEO conjugates for solubilization of *m*-THPC A) and UV–Vis absorption spectra solubilized *m*-THPC in water with peptide-PEO conjugates (**PI** and **PII**) as well as reference experiments B) Conditions: *c*[conjugates] = 15 μm in water, rt, pH 7, *c*[*m*-THPC] = 3.6 μm (**PI**)/8.2 μm (**PII**).

established lyophilization/dissolution procedure.[35] As it could be expected, the highly hydrophobic **PII** exhibited the highest drug payload capacity with 127 mg drug per gram carrier (1:1.8 molar drug to carrier ratio). **PI** solubilized noticeably less *m*-THPC, reaching with 55 mg drug per gram carrier a significantly smaller molar drug to carrier ratio of 1:5.7. The differences in payload capacity might be a consequence of the polar Gln residue positioned in the center of the N-terminal tetramer segment of **PI**.

To elucidate the important interactions on the molecular level between peptide sequences and *m*-THPC drug that lead to significant differences in solubilization capacities a computationally accessible model system was investigated *in silico*. The software MOLOC[44] was used to model idealized 1:1 complexes of *m*-THPC and peptides **PI** and **PII** (omitting the PEO moiety). Figure 3 shows for both cases a preferential disposition of the peptides around *m*-THPC, resulting in a sandwich-type complex, in which the peptide wraps around *m*-THPC. Numerous hydrophobic contacts, especially face-to-face and edge-to-face π–π interactions, are believed to be the dominant cargo–transporter interactions. In addition, amide–π stacking interactions are also observed. Owing to the flexible, central disulfide linker, neither inter- or intramolecular clashes nor unfavorable conformations are observed. Nevertheless, the torsion angle of the disulfide bond has been checked after every energy optimization to be within the preferred range for this moiety found in similar fragments in the Cambridge Structural Database.[45] The computational model systems suggest that for **PI** and **PII**, the formation of favorable H bonds with the phenolic groups of *m*-THPC anchors the peptide to the *m*-THPC. Whenever hydrophobic residues are not involved in direct interactions with *m*-THPC, they are engaged in intramolecular hydrophobic contacts, contributing indirectly to the stabilization of the complex. Compact complexes have been modeled for **PII**, whereas **PI**/*m*-THPC complexes seem to be less tightly packed as Gln, the third amino-acid residue of **PI**, is solvent-exposed and does not bind to *m*-THPC. Taking the dimensions of the drug and the peptide strand into account as well as the results of

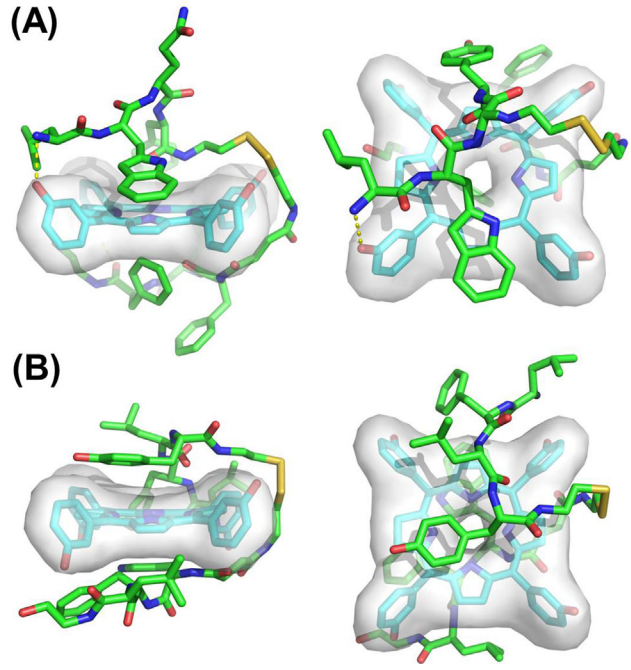

Figure 3. Molecular modeling studies of *m*-THPC bound to peptide sequences of bioconjugates **PI** and **PII** in an idealized 1:1 complex: I/*m*-THPC A) and II/*m*-THPC B) in side (left) and top view (right). The van der Waals surface of *m*-THPC is shown as gray envelope of blue stick model and the peptide sequences are shown as green stick models. Figure was generated with the software Pymol.[46]

the solubilization studies, a stoichiometric 1:1 complex formation between drug and host peptide is unlikely to occur. However, the modeling studies can provide insights into relevant interaction modes between peptide functionalities and the drug moiety to illustrate how the cargo is bound non-covalently by the carrier peptides.

Further insight into the aggregation states was provided by dynamic light scattering (DLS) by analyzing solutions of each of the bioconjugates (**PI** and **PII**) with and without *m*-THPC, as well as prior and after treatment with tris(2-carboxyethyl) phosphine to chemically cleave the disulfide linkers (cf. S.I. Table S3). In aqueous solution in the absence of *m*-THPC, **PI** and **PII** form aggregates with hydrodynamic radii (R_h) of 30–60 nm. This was to be expected as the selected amino acid sequences are dominated by hydrophobic residues, leading to amphiphilic PEO–peptide conjugates. Considering the hydrophobicity and the molecular dimensions of *m*-THPC it is logically that *m*-THPC loading increased the size of aggregation of **PI** and **PII** to $R_h = 200 \pm 10$ nm and 90 ± 6 nm, respectively. Interestingly, reductive cleavage of the cystamine disulfide bonds leads to a minor reduction of **PI**/*m*-THPC complex size to $R_{h,\ \mathbf{PI}/\mathrm{THPC;TCEP}} = 160 \pm 13$ nm, whereas similar conditions lead to a significant decrease of **PII**/*m*-THPC complex size to $R_{h,\ \mathbf{PII}/\mathrm{THPC;TCEP}} = 45 \pm 5$ nm.

3.4. Drug Trans-Solubilization and Activation

m-THPC was packed in the core of the aggregates and fluorophore quenching occurs in both **PI** and **PII** solubilizer systems. Previously, it could be shown that fluorescence quenching of *m*-THPC in congener solubilizer systems goes along with the loss of the capability to generate singlet oxygen upon irradiation.[35] Inactivation of the sensitizer in a silent transport state, in fact, might be highly beneficial as undesired toxicity could be diminished and shelf-life-time increased. Taking into account that *m*-THPC transfers in blood rapidly to plasma proteins,[47] the drug trans-solubilization from the silent **PI**/*m*-THPC and **PII**/*m*-THPC complexes toward bovine serum albumin (BSA) was studied as an appropriate model (cf. Figure 4). With drug transfer to BSA the fluorescence quenching was successively reduced, setting *m*-THPC in the pharmacologically active state that allowed singlet oxygen generation. Hence, the increase of the fluorescence over time is a suitable measure to follow cargo release and drug activation kinetics. The cargo trans-solubilization from *m*-THPC-loaded bioconjugates **PI** and **PII** to alkylated BSA ($BSA^{alkylated}$)[48] was studied initially before reductive cleavage of the disulfide linkers in the solubilizers. 10 μM $BSA^{alkylated}$ was added to two different solutions containing 0.1 μM *m*-THPC solubilized by either **PI** or **PII**. Figure 4 shows that non-activated cargo release profiles strongly depend on the sequence. Where fluorescence increase from **PII**/*m*-THPC complexes reached ≈75% of the maximum within 1 h and practically levels off after 4 h, the release from **PI**/*m*-THPC complexes occurred much more slowly and showed significant increase over the entire 18 h period that was investigated. Moreover, from non-activated transporter–drug complexes of **PI** only ≈75% of the *m*-THPC activity that was reached by the **PII**/drug complexes developed during trans-solubilization. Probably this is a consequence of the higher solubilizer to drug ratio of **PI**/*m*-THPC that leads to bigger aggregates, which more effectively stabilize the drug in the core of the drug/carrier complex. However, the drug activation profiles observable after disulfide cleavage significantly changed and thus reveal an impact of carrier cleavage on drug release kinetics from *m*-THPC-loaded bioconjugates. Prior to the trans-solubilization experiments, the solutions of both bioconjugates solubilizing 0.1 μM *m*-THPC were treated with an excess of *tris*(2-carboxyethyl)phosphine (TCEP) (5 mM). This leads to a reductive cleavage of the disulfide linkers as was confirmed by HPLC measurements (cf. S.I. Figure S3). Drug trans-solubilization to 10 μM $BSA^{alkylated}$ was followed by fluorescence spectroscopy. Comparison of drug-activation kinetics of reduced with non-reduced samples revealed two different behaviors, where the polarity of the formed peptide fragments seems to play an important role (Figure 4). The reductive cleavage of **PI** accelerates the

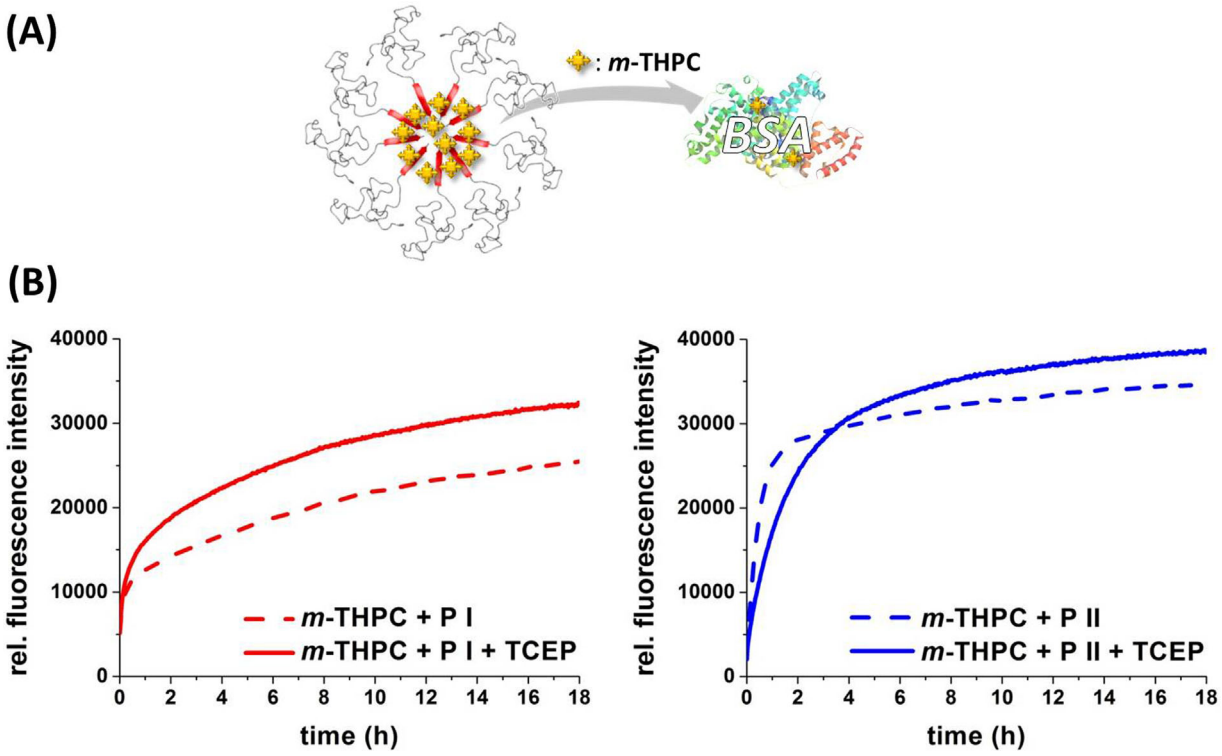

Figure 4. A) Schematic representation of drug/bioconjugate aggregate formation and drug trans-solubilization to BSA. B) Drug release and activation kinetics measured by fluorescence emission over time of *m*-THPC/solubilizer complexes (**PI**–II) in the presence of $BSA^{alkylated}$ with (line) and without (dashes) conjugate cleavage by TCEP. Conditions: (b) $\lambda_{ex} = 417$ nm, $\lambda_{em} = 653$ nm, [BSA] = 10 μm, [*m*-THPC] = 0.1 μm, [TCEP] = 5 mm.

development of fluorescently active *m*-THPC species under trans-solubilization conditions, leading to faster drug activation and improved amounts of activated drug by 20%. **PI**/*m*-THPC complexes activate after TCEP treatment within 2 h 75% of the *m*-THPC amounts that are released within 18 h from non-cleaved complexes. As opposed to this acceleration, the development of active *m*-THPC species from reduced **PII**/*m*-THPC complexes showed initial retardation when compared to the profile prior to reduction (cf. Figure 4). Interestingly, fluorescence kinetics of the reduced **PII**/*m*-THPC samples start with lower rates (Figure 4). After 3.5 h, both traces cross and finally level off at values where the reduced sample is 10% more fluorescent than the non-reduced one.

Fluorescence spectroscopy and DLS suggested that **PI**/*m*-THPC forms bigger aggregates, which exhibit improved trans-solubilization to BSA upon reduction. The opposite effect could be observed for **PII**/*m*-THPC, showing smaller aggregates and a retardation of the trans-solubilization upon reductive cleavage. Taking the chemical similarities in the peptide sequences of **PI** and **PII** into account, glutamine as single polar amino acid found in **PI** could explain the solubilization capacity as well as activated and non-activated trans-solubilization.

Mechanistically, TCEP cleavage of **PI** results in two fragments composed of an FFF-*block*-PEO and the water-soluble peptide LWQY. As the latter segment probably leaves the **PI**/*m*-THPC complex after TCEP treatment due to its hydrophilicity, an accelerated trans-solubilization is reasonable. In contrast to this, cleavage of **PII** generates water-insoluble peptide segments with hydrophobic LFLY sequences and an amphiphilic WFL-*block*-PEO. These fragments contribute both to *m*-THPC stabilization in cleaved **PII**/*m*-THPC complexes. The observed decrease in trans-solubilization rates might be rationalized by more proper adjutant of carrier segment/drug interactions due to the increased degree of freedom by the cystamine cleavage. This mechanism is corroborated by the observation that the size of **PII**/*m*-THPC complexes is reduced significantly upon TCEP treatment in the absence of BSA.

4. Conclusion

A generic method to tailor-made switchable peptide sequences as solubilizers for the photosensitizer *m*-THPC was established. Suitable peptide sequences could be selected from large one bead/one component peptide

libraries. The possibility to tune drug-release kinetics was implemented into the screening process, by positioning a cystamine-based amino acid derivative on a fixed central position of the peptide library in-between two sequentially variable segments. Fluorescence microscopy was used to follow the partitioning of the drug in the library and MALDI-ToF-MS/MS sequencing revealed a set of binding peptides, which were integrated into peptide-*block*-poly(ethylene oxide) bioconjugates. The resulting tailor-made peptide-PEO solubilizers allowed for sequence-specific, non-covalent binding, and solubilization of *m*-THPC. Drug-transfer kinetics toward blood plasma protein models could be modulated by reductive cleavage of the cystamine disulfide segment. Solubilization efficiencies, drug trans-solubilization rates, and drug activation kinetics in response to the cleavage upon disulfide reduction were studied and strong dependencies on the amino acid sequence of the bioconjugate were found. These results highlight the advantages and possibilities arising from tailored peptide–polymer conjugates to render hydrophobic drugs water soluble. These specific drug solubilizers offer precisely tunable, small-molecule binding and adjustable activation/release kinetics by altering peptide sequences. Certainly, an improved binding strength is required to translate the concept from solubilizers to transporters. However, conceptionally the accelerated cargo release of the drug through an external trigger might occur upon cellular uptake by facing the reductive intercellular environment, offering a valuable strategy to be exploited in the future.

Acknowledgements: The authors acknowledge M. Senge (Trinity College Dublin) and B. Röder (HU) for providing *m*-THPC, H. Stephanowitz (FMP) for MS sequencing and K. Linkert (HU) for peptide synthesis. Funding was granted from the European Research Council under the European Union's 7th Framework Program (FP07-13)/ERC Starting grant "Specifically Interacting Polymers – SIP" (ERC 305064) (HGB) as well as The Netherlands Organisation for Scientific Research (NWO-CW, VENI grant) and from the Ministry of Education, Culture and Science (gravitation program 024.001.035) (AKHH). D. P. and L. H. thank the DFG for funding through the Emmy Noether Program HA 5950/1-1.

Received: October 8, 2014; Published online: January 01, 2014; December 29, 2014; DOI: 10.1002/mabi.201400443

Keywords: drug delivery; drug formulation; PEG; peptide; stimuli responsive

[1] H. D. Williams, N. L. Trevaskis, S. A. Charman, R. M. Shanker, W. N. Charman, C. W. Pouton, C. J. H. Porter, *Pharmacol. Rev.* **2013**, *65*, 315.
[2] T. Kennedy, *Drug Discovery Today* **1997**, *2*, 436.
[3] K. H. Bleicher, H. J. Bohm, K. Muller, A. I. Alanine, *Nat. Rev. Drug Discov.* **2003**, *2*, 369.
[4] W. L. Jorgensen, *Science.* **2004**, *303*, 1813.
[5] J.-H. Zhang, T. D. Y. Chung, K. R. Oldenburg, *J. Biomol. Screen.* **1999**, *4*, 67.
[6] S. Thaisrivongs, M. N. Janakiraman, K.-T. Chong, P. K. Tomich, L. A. Dolak, S. R. Turner, J. W. Strohbach, J. C. Lynn, M.-M. Horng, R. R. Hinshaw, K. D. Watenpaugh, *J. Med. Chem.* **1996**, *39*, 2400.
[7] C. A. Lipinski, F. Lombardo, B. W. Dominy, P. J. Feeney, *Adv. Drug Delivery Rev.* **2012**, *64*, 4.
[8] S. Dunne, B. Shannon, C. Dunne, W. Cullen, *BMC Pharmacol. Toxicol.* **2013**, *14*, 2050.
[9] S. M. Paul, D. S. Mytelka, C. T. Dunwiddie, C. C. Persinger, B. H. Munos, S. R. Lindborg, A. L. Schacht, *Nat. Rev. Drug. Discov.* **2010**, *9*, 203.
[10] H. Ringsdorf, *J. Polym. Sci: Polym. Symp.* **1975**, *51*, 135.
[11] D. V. Santi, E. L. Schneider, R. Reid, L. Robinson, G. W. Ashley, *Proc. Natl. Acad. Sci. USA* **2012**, *109*, 6211.
[12] R. Duncan, *Nat. Rev. Drug Discov.* **2003**, *2*, 347.
[13] S. Gopinathan, A. Nouraldeen, A. G. E. Wilson, *Future Med. Chem.* **2010**, *2*, 1391.
[14] G. Riess, *Prog. Polym. Sci.* **2003**, *28*, 1107.
[15] A. Kuksal, A. Tiwary, N. Jain, S. Jain, *AAPS PharmSciTech* **2006**, *7*, E1.
[16] M. Buonaguidi, V. Carelli, G. Di Colo, E. Nannipieri, M. F. Serafini, *Int. J. Pharm.* **1997**, *147*, 1.
[17] R. J. Amir, S. Zhong, D. J. Pochan, C. J. Hawker, *J. Am. Chem. Soc.* **2009**, *131*, 13949.
[18] M. S. Yavuz, Y. Cheng, J. Chen, C. M. Cobley, Q. Zhang, M. Rycenga, J. Xie, C. Kim, K. H. Song, A. G. Schwartz, L. V. Wang, Y. Xia, *Nat. Mater.* **2009**, *8*, 935.
[19] S. Kim, K. E. Healy, *Biomacromolecules* **2003**, *4*, 1214.
[20] S. K. Choi, M. Verma, J. Silpe, R. E. Moody, K. Tang, J. J. Hanson, J. R. J. Baker, *Bioorg. Med. Chem.* **2012**, *20*, 1281.
[21] G. Leriche, L. Chisholm, A. Wagner, *Bio. Med. Chem.* **2012**, *20*, 571.
[22] Y. Kakizawa, A. Harada, K. Kataoka, *J. Am. Chem. Soc.* **1999**, *121*, 11247.
[23] H. G. Börner, *Prog. Polym. Sci.* **2009**, *34*, 811.
[24] D. Lowik, E. H. P. Leunissen, M. van den Heuvel, M. B. Hansen, J. C. M. van Hest, *Chem. Soc. Rev.* **2010**, *39*, 3394.
[25] P. Wilke, N. Helfricht, A. Mark, G. Papastavrou, D. Faivre, G. H. Börner, *J. Am. Chem. Soc.* **2014**, *136*, 12667.
[26] T. Schwemmer, J. Baumgartner, D. Faivre, H. G. Börner, *J. Am. Chem. Soc.* **2011**, *134*, 2385.
[27] C. M. Kolodziej, S. H. Kim, R. M. Broyer, S. S. Saxer, C. G. Decker, H. D. Maynard, *J. Am. Chem. Soc.* **2012**, *134*, 247.
[28] C. Stutz, I. Bilecka, A. F. Thunemann, M. Niederberger, H. G. Börner, *Chem. Commun.* **2012**, *48*, 7176.
[29] P. Wilke, H. G. Börner, *ACS Macro Lett.* **2012**, *1*, 871.
[30] B. Apostolovic, S. P. E. Deacon, R. Duncan, H. A. Klok, *Biomacromolecules* **2010**, *11*, 1187.
[31] L. A. Canalle, D. Lowik, J. C. M. van Hest, *Chem. Soc. Rev.* **2010**, *39*, 329.
[32] R. Gentsch, F. Pippig, K. Nilles, P. Theato, R. Kikkeri, M. Maglinao, B. Lepenies, P. H. Seeberger, H. G. Börner, *Macromolecules* **2010**, *43*, 9239.
[33] H. G. Börner, *Macromol. Rapid Commun.* **2011**, *32*, 115.
[34] A. K. H. Hirsch, F. Diederich, M. Antonietti, H. G. Borner, *Soft Matter* **2010**, *6*, 88.
[35] S. Wieczorek, E. Krause, S. Hackbarth, B. Röder, A. K. H. Hirsch, H. G. Börner, *J. Am. Chem. Soc.* **2013**, *135*, 1711.
[36] M. O. Senge, J. C. Brandt, *Photochem. Photobiol.* **2011**, *87*, 1240.
[37] C. Hopper, A. Kübler, H. Lewis, I. B. Tan, G. Putnam, G. the Foscan 01 Study, *Intern. J. Cancer* **2004**, *111*, 138.

[38] M. O. Senge, *Photodiagnosis and Photodynamic Therapy* **2012**, *9*, 170.
[39] L. Hartmann, S. Häfele, R. Peschka-Süss, M. Antonietti, H. G. Börner, *Macromolecules* **2007**, *40*, 7771.
[40] D. Ponader, F. Wojcik, F. Beceren-Braun, J. Dernedde, L. Hartmann, *Biomacromolecules* **2012**, *13*, 1845.
[41] K. S. Lam, S. E. Salmon, E. M. Hersh, V. J. Hruby, W. M. Kazmierski, R. J. Knapp, *Nature* **1991**, *354*, 82.
[42] E. Gross, "[27] The cyanogen bromide reaction", in *Methods in Enzymology* (Eds: C.H.W. Hirs), Academic Press, **1967**, p. 238.
[43] J. Seidler, N. Zinn, M. E. Boehm, W. D. Lehmann, *Proteomics* **2010**, *10*, 634.
[44] P. Gerber, K. Müller, *J. Comput. -Aided Mol. Des.* **1995**, *9*, 251.
[45] F. Allen, *Acta Crystallogr., Sect. B: Struct. Sci., Cryst. Eng. Mater.* **2002**, *58*, 380.
[46] V.S. The PyMOL Molecular Graphics System, LLC.
[47] S. Sasnouski, V. Zorin, I. Khludeyev, M.-A. D'Hallewin, F. Guillemin, L. Bezdetnaya, *Biochim. Biophys. Acta* **2005**, *1725*, 394.
[48] Z. Zmatliková, P. Sedláková, K. Lacinová, A. Eckhardt, S. Pataridis, I. Mikšík, *J. Chromatogr. A* **2010**, *1217*, 8009.